Basic Res Cardiol (2015) 110:56
DOI 10.1007/s00395-015-0515-4

ORIGINAL CONTRIBUTION

Regulatory role of CARD3 in left ventricular remodelling and dysfunction after myocardial infarction

Liangpeng Li[1] · Xiaodi Wang[1] · Wen Chen[1] · Haoyu Qi[1] · Ding-Sheng Jiang[2,3] · Ling Huang[2,3] · Fuhua Huang[1] · Liming Wang[1] · Hongliang Li[2,3] · Xin Chen[1]

Received: 7 October 2014 / Accepted: 6 October 2015 / Published online: 13 October 2015

Abstract Caspase activation and recruitment domain 3 (CARD3) is a caspase recruitment domain (CARD)-containing serine/threonine kinase and plays a pivotal role in apoptosis, immunity, tissue development and proliferation. To date, the causal relationship between CARD3 and myocardial infarction (MI) remains largely unexplored. This study aimed to identify the functional significance of CARD3 in the regulation of cardiac remodelling after MI and the underlying mechanisms of its effects. The levels of CARD3 expression were up-regulated in failing human and mouse post-infarction hearts. In addition, CARD3-knockout (KO) mice and transgenic mice overexpressing CARD3 in the heart were then generated and subjected to MI. Compared with wild-type (WT) control mice, CARD3-KO mice developed smaller infarct sizes, improved survival rates, and preserved left ventricle (LV) function after MI. Significantly, CARD3-KO hearts had less cardiomyocyte apoptosis and inflammatory cell infiltration in the infarct border zone. Attenuated LV remodelling was also observed in the KO hearts following MI, with reduced cardiac hypertrophy and fibrosis. Conversely, CARD3 overexpression resulted in the opposite MI-induced phenotype. Similar results were observed in ex vivo-cultured neonatal rat cardiomyocytes exposed to hypoxia. Mechanistically, we discovered that the CARD3-mediated detrimental effects of MI were associated with the activation of the NF-κB and p38 signalling cascades. Taken together, these data demonstrate that CARD3 serves as a novel positive modulator of ventricular remodelling after MI via the regulation of the NF-κB and p38 signalling. Thus, CARD3 may be a promising therapeutic target for the treatment of heart failure after MI.

Keywords CARD3 · Myocardial infarction · Cardiac remodelling · NF-κB · p38

Introduction

Myocardial infarction (MI) remains a significant and unsolved health problem that seriously affects the human health throughout the world [11, 13]. After the acute phase of MI, a chronic maladaptive phase of ventricular remodelling occurs. This phase is associated with irreversible cardiomyocyte apoptosis, inflammation, fibrosis, and hypertrophy, leading to the development of ventricular dilatation, impaired systolic function, congestive heart failure and death [37, 46]. Ventricular remodelling may continue for weeks or months until the distending forces are counterbalanced by the tensile strength of the collagen scar [15, 51]. Preventing left ventricular (LV) remodelling after MI is of highly desirable as it may be related to a reduction in adverse cardiac events, including a decreased exacerbation of congestive heart failure and fewer cardiac mortality rates [22]. Therefore, it is of critical importance

Electronic supplementary material The online version of this article (doi:10.1007/s00395-015-0515-4) contains supplementary material, which is available to authorized users.

✉ Xin Chen
stevecx@njmu.edu.cn

[1] Department of Thoracic and Cardiovascular Surgery, Nanjing Hospital Affiliated to Nanjing Medical University, Changle Road 68, Nanjing 210006, Jiangsu, People's Republic of China

[2] Department of Cardiology, Renmin Hospital of Wuhan University, Wuhan 430060, People's Republic of China

[3] Cardiovascular Research Institute of Wuhan University, Wuhan 430060, People's Republic of China

to explore the novel mechanisms for this maladaptation and to develop therapeutic strategies that are effective in preventing LV remodelling.

CARD3, also known as RIP2, CARDIAK, and RICK, is a 61-kDa adaptor protein that belongs to the CARD family and contains an N-terminal serine/threonine kinase domain and a C-terminal CARD [23]. Several analyses have revealed that CARD3 is activated in a variety of cell death paradigms [32]. For instance, Zhang et al. [58] recently reported that CARD3 plays a key role in regulating caspase-1 apoptotic activity in neurons. Moreover, overexpression of CARD3 induces apoptosis in several cell lines, such as human embryonic kidney cells and MCF7 breast cancer cells [41]. Notably, an abrupt augmentation in cardiomyocyte apoptosis was observed in ischemic hearts following MI. Apoptosis has also been proposed as an important mechanism for the elimination of cardiomyocytes after MI [7]. Moreover, previous studies have demonstrated that CARD3 interacts with members of both TLRs (Toll-like receptors) and Nods (nucleotide oligomerisation domains) to mediate signalling for receptors of the innate and adaptive immune systems [38]. The stimulation of Nod1 or Nod2 by their specific bacterial activators triggers the recruitment of CARD3 and the association of CARD3 with Nod1 or Nod2 via CARD–CARD interactions [18]. In addition, cytokine production in CARD3-deficient macrophages were clearly reduced when TLRs were stimulated with lipopolysaccharide, peptidoglycan as well as double-stranded RNA [21], indicating that CARD3 may play a pivotal role in inflammatory response. Furthermore, abundant evidence has shown that MI is associated with inflammatory responses, which can extend myocardial injury [35]. More importantly, CARD3 is also expressed ubiquitously in various adult tissues, including the heart [33]. Despite the functional role of CARD3 in apoptosis and inflammation, there have been no studies regarding the pathophysiological contribution of CARD3 expression to the development of cardiac remodelling following MI and the progression to heart failure. Therefore, it is necessary to determine the consequence of overexpression and ablation of CARD3 in the heart after MI.

Our preliminary studies demonstrate for the first time that CARD3 expression is strongly induced in infarcted murine myocardium and in LV tissue samples obtained from patients with ischemic heart disease (IHD). We further report that MI-induced cardiac remodelling is exaggerated in CARD3-overexpressing mice, whereas it is limited in CARD3-deficient mice. Lastly, our data revealed that CARD3-mediated post-MI remodelling via activation of the NF-κB and p38 signalling pathway. These findings clearly demonstrate that CARD3 may be indispensable in the development of cardiac remodelling after MI, and that the use of CARD3 gene therapy may be an effective strategy for protection against post-MI cardiac remodelling and heart failure.

Materials and methods

Animals

All of surgical procedures and protocols were approved by the Animal Care and Use Committee of Nanjing Medical University and confirmed to the Guide for the Care and Use of Laboratory Animals published by the US National Institutes of Health (NIH Publication No. 85-23, revised 1996). Transgenic (TG) mice were generated with full-length mouse CARD3 cDNA under the control of the α-myosin heavy chain (α-MHC) promoter. The transgenic mice (C57BL/6J background) were created by microinjecting the α-MHC-CARD3 construct into fertilised mouse embryos, and the animals were identified via PCR analysis of tail genomic DNA. The primers used were 5′-ATCTCCCCCATAAGAGTTTGAGTC-3′ and 5′-CCAAGAGCAATTTCATGCAG-3′. Four independent transgenic lines were established and studied.

The CARD3-knockout (KO) mice were kindly provided by Dr Richard Flavell (Howard Hughes Medical Institute, Yale University, New Haven, Connecticut). Eight- to ten-week-old male CARD3-KO, CARD3-TG and control (WT littermates and non-transgenic) mice were used in all studies. All of the animals were housed in an environment with controlled light cycles (12 h light/12 h dark), temperature, and humidity; food and water were provided ad libitum. All of the surgeries and subsequent analyses were performed in a blinded fashion.

Mouse MI model

Ligation of the left anterior descending (LAD) coronary artery was performed in 8- to 10-week-old mice, as described with minor modifications [24, 53]. Briefly, the animals (23–27 g body weight) were anesthetised by intraperitoneal injection of pentobarbital sodium (50 mg/kg), and the adequacy of anaesthesia was monitored during the surgical procedures by the lack of the pedal withdrawal reflex, slow constant breathing, and no response to surgical manipulation. Buprenorphine (0.1 mg/kg, SC) was administered for post-operative analgesia. The animals were then intubated with a 20-gauge polyethylene catheter and ventilated with room air using a rodent ventilator (model VFA-23-BV, Kent Scientific, USA). After completion of a thoracotomy in the third or fourth intercostal space, the pericardium was opened, and the proximal left coronary descending (LAD) artery under the tip of the left

atrial appendage was encircled and ligated using a 7–0 proline suture. Lastly, the chest wall was closed. The animals remained in a supervised setting until fully conscious. In sham-operated animals, the left coronary artery was encircled but not ligated. There is a high mortality associated with this experimental model, and animals that died within 24 h of surgery were excluded from the analysis. In our study, the MI surgery was performed by the technician who has made the MI model more than 5 years in our institute, and all the experiments were performed in accordance with the randomised, double-blind, parallel mouse group. Moreover, we have performed Evans blue staining to check whether the site of ligature is consistent (Supplemental Figure S1). Accordingly, the heart sections of KO and TG mice after MI surgery are located in the concordant ligation sites.

Echocardiography and haemodynamic evaluation

Echocardiographic and haemodynamic measurements were performed as described previously [20, 25]. Mice were anesthetised with 1.5–2 % isoflurane by inhalation, and then echocardiography was then performed using a MyLab30CV ultrasound (Biosound Esaote Inc.) with a 10-MHz linear array ultrasound transducer. The left ventricle (LV) was assessed in both parasternal long-axis and short-axis views at a frame rate of 120 Hz. Left ventricular end-diastolic diameter (LVEDD), left ventricular end-systolic diameter (LVESD), and LV wall thickness were measured from M-mode tracings with a sweep speed of 50 mm/s at the mid-papillary muscle level. End-systole or end-diastole phases corresponded to the smallest or largest LV diameters, respectively. Echocardiographic measurements were taken on M-mode in triplicate from more than 3 separate mice per group.

For the haemodynamic analyses, a 1.4-F Millar microtip catheter transducer (SPR-839, Millar Instruments, Houston, Texas) was inserted into the right carotid artery and advanced into the LV under pressure control. After stabilisation for 15 min, pressure signals and heart rates were recorded continuously with an ARIA pressure–volume conductance system coupled with a Powerlab/4SP A/D converter, stored, and then displayed on a personal computer. PVAN software (Millar Instruments) was used for subsequent analysis of pressure–volume loops.

Morphological examination and infarct size measurement

At different time points after surgery, mice were anaesthetised intraperitoneally using sodium pentobarbital (100 mg/kg) and killed by swift decapitation according to the Guide for the Care and Use of Laboratory Animals published by the United States National Institutes of Health. The hearts were excised and fixed with a 10 % solution of formalin in PBS. Subsequently, the hearts were embedded in paraffin and cut serially from the apex to the base. Each short-axis section (5 μm) was stained with hematoxylin and eosin (H&E) for morphometric analysis. To measure the myocardial infarct size, the initial research have compared 3 methods, respectively, based on (1) infarct area, (2) epicardial and endocardial infarct arc lengths, and (3) midline infarct arc length in a mouse chronic infarction model. Importantly, the estimation of infarct midlines is a simple and reliable approach to determine infarct size. Accordingly, in our present study, to assess the infarct size, the mouse hearts were sectioned transversely at 5 μm after dehydration and paraffin embedding. Slices, stained with hematoxylin and eosin (H&E), were collected with an interval of 300 μm between each section. As shown in Supplemental Fig S2, the LV myocardial midline was marked with the broken white line at the center between the epicardial (red) and endocardial (green) surfaces and the length of the midline was measured as midline circumference. Midline infarct length (blue arrow line) was taken as the midline of the length of infarct. Infarct size derived from midline length measurement was calculated by dividing the sum of midline infarct lengths by the sum of midline circumferences from all sections and multiplying by 100. The infarcted area of the left ventricle was obtained using a quantitative digital image analysis system (Image-Pro Plus 6.0). The infarct size (%) was calculated as a percentage of the total LV wall circumference from each of the 3 LV sections. All measurements were made in a blinded fashion.

To assess myocyte cross-sectional area (CSA) and myocardial fibrosis, sections were stained for membranes with hematoxylin and eosin (H&E) and picrosirius red-stained (PSR), respectively. In each group, more than 100 LV myocytes were examined as described previously [25]. Single myocytes and fibrillar collagen were visualised by microscopy and were measured using a quantitative digital image analysis system (Image-Pro Plus 6.0).

Immunofluorescent staining

To identify inflammatory cell infiltration, the sections were stained according to standard immunofluorescence staining techniques. Briefly, the mice were anaesthetised with sodium pentobarbital (100 mg/kg), and the hearts were rapidly excised and fixed with a 10 % solution of formalin in PBS. Thereafter, the hearts were paraffin embedded and cut into 5-μm sections. The heart sections were dried, dewaxed, hydrated, and repaired in high pressure (100 mm Hg). Subsequently, these sections were washed in PBS, sealed with 10 % sheep serum, and incubated at 4 °C

overnight with the following primary antibodies: rabbit anti-CD3 (1:100 dilution, ab16669, Abcam), rat anti-Ly6G (1:100 dilution, 551459, BD Biosciences), and rabbit anti-Mac1 (CD11b, 1:100 dilution, ab75476, Abcam). After being washed in PBS, the sections were incubated with the indicated secondary antibodies for 1 h at room temperature and subsequently washed in PBS. The following secondary antibodies were used: donkey anti-rabbit IgG(H + L) Alexa Fluor® 568 (A10042; Invitrogen), and goat anti-rat IgG(H + L) Alexa Fluor® 568 (A11077; Invitrogen). The nuclei were stained with 4′,6-diamidino-2-phenylindole (DAPI; S36939, Invitrogen). The images were acquired with a fluorescence microscope (OLYMPUS DX51) and DP2-BSW software (version 2.2). Quantitative assessments for CD3, Mac-1 and Ly6G-positive cells were performed, and the number of positive cells in 3–5 randomly selected fields of the infarct border zone was calculated for each heart using a quantitative digital image analysis system (Image-Pro Plus 6.0) by at least two independent investigators.

Determination of cell death

The terminal deoxynucleotidyl transferase-mediated dUTP nick-end labelling (TUNEL) assay was used to monitor the extent of DNA fragmentation as a measure of apoptosis. The assay was performed in sections with ApopTag® Plus In Situ Apoptosis Fluorescein Detection Kit (S7111, R&D Systems, Minneapolis, USA) according to the manufacturer's recommendations. The TUNEL-positive cells in the infarct border zone were observed using a fluorescent microscope. More than four fields in the infarct border zone on each slide were randomly examined and quantified under high-power magnification (400).

Cultured NRCMs were treated with the indicated adenoviruses for 24 h and then stimulated with hypoxia for the indicated times. To detect apoptosis or necrosis, the cells were fixed with 4 % paraformaldehyde, and were rinsed with PBS. Subsequently, the cells were incubated for 10 min with Hoechst 33258 (H3567, Invitrogen; 10 μg/ml) and stained with propidium iodide (PI) (P4864, Sigma-Aldrich; 15 μg/ml) for 15 min, after which they were observed under a fluorescent microscope. Cell viability is presented as the number of dead cells (PI-staining)/the total number of cells (Hoechst 33258-staining).

Quantitative real-time RT-PCR and western blot analyses

Quantitative real-time PCR and western blotting were performed as previously described [3, 27]. Briefly, total RNA was extracted from ventricles and cultured cardiomyocyte using a TRIzol reagent (Invitrogen) and reverse-transcribed into cDNA using oligo (dT) primers with a Transcriptor First Strand cDNA Synthesis Kit (Roche, 04896866001). PCR amplifications were quantified using the SYBR Green PCR Master Mix (Applied Biosystems) and normalised to GAPDH gene expression. The real-time PCR primers that were used are shown in Supplementary Table S1.

For western blotting, cardiac tissue and primary myocyte cells were lysed using a RIPA buffer, and the protein concentration was examined with a BCA protein assay kit (Pierce; Rockford, IL, USA). Protein extracts (50 μg) were separated by SDS-PAGE (Invitrogen, NP0301BOX) and were electrotransferred to PVDF membrane (Millipore, IPVH00010) that was blocked in TBS containing 5 % skim milk powder for 90 min at room temperature. The membrane was incubated with a peroxidase-conjugated secondary antibody [Peroxidase-affinipure goat anti-mouse IgG (H + L) (115-035-003) or Peroxidase-affinipure goat anti-rabbit IgG (H + L) (111-035-003); Jackson ImmunoResearch Laboratories]. Antibodies against the following proteins were purchased from Cell Signaling Technology (Danvers, MA, USA): CARD3 (#4982), MEK1/2 (#9122), phospho-MEK1/2 (#9154), ERK1/2 (#4695), phospho-ERK1/2 (#4370), JNK1/2 (#9258), phospho-JNK1/2 (#4668), p38 (#9212), phospho-p38 (#4511), P65 (#4764), phospho-P65 (#3033), IκBα (#4814), phospho-IκBα (#9246), Bid (#2003), Bak (#3814), Caspase 3 (#9662), cleaved Caspase 3 (#9661). The GAPDH (MB001) antibody was purchased from Bioworld Technology (Harrogate, UK). A FluorChem E (Cell biosciences) imaging system was used to visualise the signals according to the manufacturer's instructions. The specific protein expression levels were normalised to GAPDH on the same nitrocellulose membrane.

Cardiomyocyte culture and infection with recombinant adenoviral vectors, and induction of hypoxia

Primary cultures of neonatal rat cardiomyocytes (NRCMs) were prepared, as described previously [25, 53]. Briefly, 1- to 2-day-old Sprague–Dawley (SD) rats which were killed by swift decapitation according to the Guide for the Care and Use of Laboratory Animals published by the United States National Institutes of Health. Cells from the hearts of these mice were seeded at a density of 1×10^6 cells/well in six-well culture plates coated with fibronectin in plating medium, which consisted of F10 medium supplemented with 10 % foetal calf serum (FCS) and penicillin/streptomycin. After 48 h, the culture medium was replaced with F10 medium containing 0.1 % FCS and BrdU (0.1 mM). FCS was purchased from HyClone (Waltham, MA, USA). The cell culture

reagents and other reagents were purchased from Sigma-Aldrich (St. Louis, MO, USA). We then infected NRCMs with AdCARD3, AdGFP, AdshCARD3, or AdshRNA at a multiplicity of infection (MOI) of 10, which yielded transgene expression without toxicity in 95–100 % of the cells. Next, the cells were exposed to hypoxia stimulation. To induce hypoxia, cultured cardiomyocytes were incubated in a Biospherix C-Chamber (model C-274, Biospherix, Redfield, New York, USA) inside a standard culture chamber. The oxygen (O_2) concentration was maintained at 5 % inside the C-Chamber, and the carbon dioxide (CO_2) concentration was maintained at 5 % by mixing a N_2 into the chamber with a ProOx 110 oxygen controller and a ProCO_2 CO_2-controller (Biospherix). Meanwhile, the control group without hypoxia, was maintained in a normal atmosphere of 5 % CO_2 and air at 37 °C.

To overexpress CARD3, the entire coding region of the rat CARD3 cDNA was subcloned into the pShuttle-cytomegalovirus (CMV) vector using the AdEasy XL Adenoviral Vector System (Stratagene). A similar adenoviral vector encoding the GFP gene was used as a control. To knockdown CARD3, AdshCARD3 adenoviruses were generated based on three rat shCARD3 constructs obtained from SABiosciences (KR54833G). The adenoviruses producing the greatest decreases in CARD3 levels were selected for further experiments. AdshRNA was selected as the non-targeting control.

Measurement of cell viability

Cell viability was assessed using Cell Counting Kit (CCK8, CW608, Donjindo), and lactate dehydrogenase (LDH) release was assessed by a colourimetric LDH cytotoxicity assay (G1782, Promega, Madison, WI), according to manufacturer's instructions.

Human heart samples

All of the procedures involving human tissue samples were approved by the Human Research Ethics Committee of Nanjing Medical University, Nanjing, China. This research conformed to the principles outlined in the Declaration of Helsinki. Informed consent was obtained from the families of prospective heart donors. Samples of failing human hearts were collected from the left ventricles of ischemia heart disease (IHD) patients undergoing heart transplants. The control samples were obtained from the left ventricles of healthy heart donors who died in accidents but whose hearts were not suitable for transplantation for non-cardiac reasons [59].

Statistical analysis

The data are presented as the mean ± SE. Differences among groups were assessed with an analysis of variance followed by a post hoc Tukey's test. Comparisons between two groups were performed using Student's t test. All statistical analyses were performed with SPSS software, version 17.0. A value of $P < 0.05$ was considered to indicate a statistically significant difference.

Results

CARD3 expression is upregulated in failing human ischemia heart disease (IHD) hearts and failing mouse post-infarction hearts

To investigate the potential role of CARD3 in the development of MI and heart failure, we first analysed whether the expression levels of CARD3 were altered in hearts with these pathological processes after MI. Both real-time PCR and Western blot assays demonstrated that in LV myocardial samples, the mRNA and protein levels of CARD3 were significantly higher in hearts collected from patients with IHD compared to normal donor hearts ($P < 0.05$ versus normal donor hearts, Fig. 1a, b). Next, we further examined CARD3 expression levels in the infarcted hearts of wild-type (WT) mice that underwent a coronary ligation or sham operation. Compared with the sham-operated hearts, CARD3 expression levels were gradually increased in the experimental mouse hearts subjected to MI from days 3 to 7. These levels remained elevated at week 4 ($P < 0.05$ versus sham operation, Fig. 1c, d). Accordingly, we have performed immunostaining in the heart sections of wild-type mice after sham or MI surgery. Our results showed that CARD3 expression level was dramatically increased in the infarct area and border zone at 1 week after MI, but no significant difference was observed in remote areas (Supplemental Fig S3). In addition, the results demonstrated that CARD3 is mainly distributed in cardiomyocytes in the heart. Taken together, the altered pattern of CARD3 expression levels in failing human hearts and mouse infarcted hearts suggested that CARD3 may be involved in post-infarction cardiac remodellling and heart failure.

Lack of CARD3 promotes survival rates, reduces infarct size, and improves cardiac function after MI

The observation of increased CARD3 expression in response to MI indicates that CARD3 may regulate

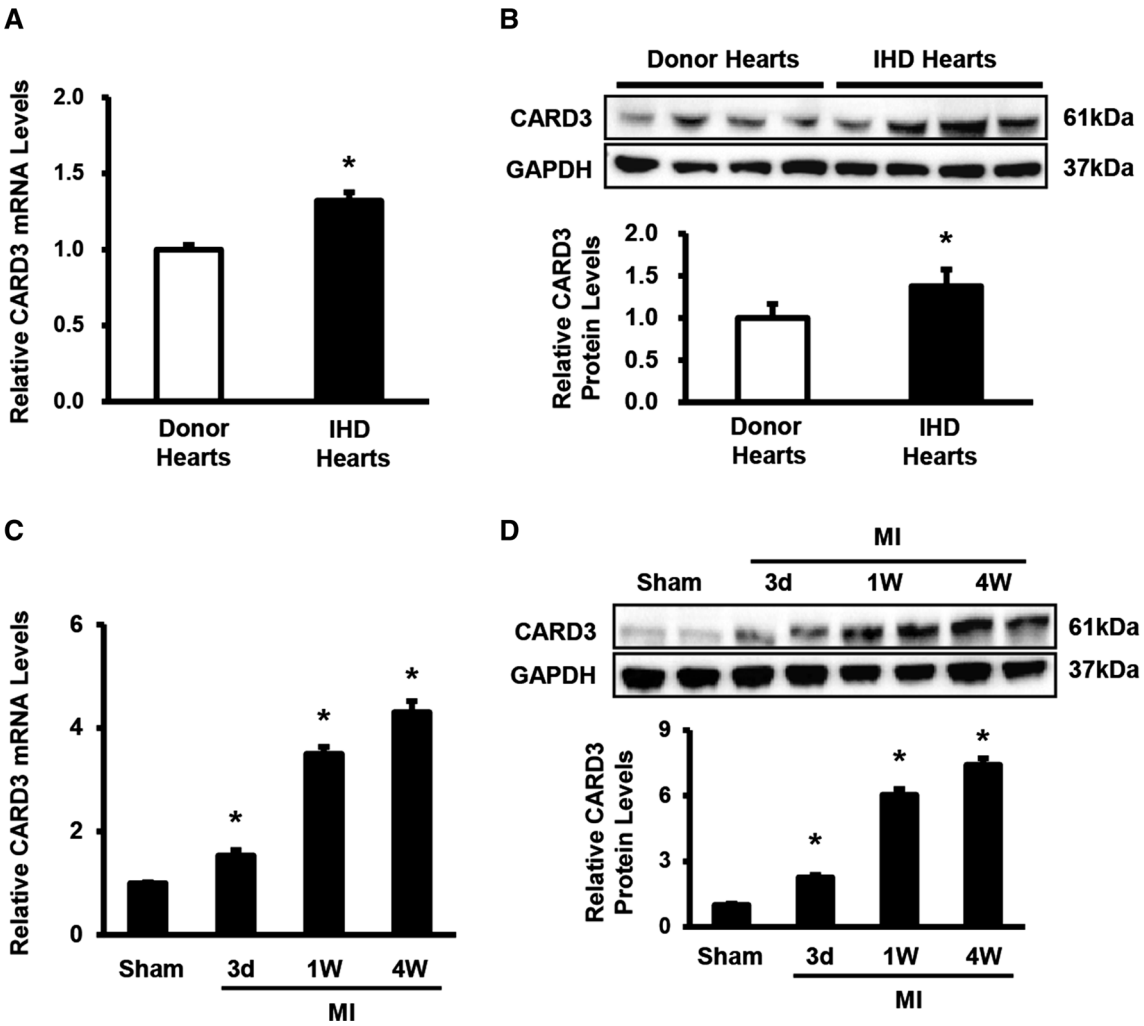

Fig. 1 CARD3 expression in failing human ischemic heart disease (IHD) hearts and failing murine post-infarction hearts. **a** Real-time PCR analyses of CARD3 mRNA levels in the left ventricles (LVs) of normal donor hearts ($n = 5$) and IHD patients ($n = 6$). *n* indicates the number of samples per experimental group, $^*P < 0.05$ versus normal donor hearts. **b** Representative western blots of CARD3 protein levels in normal donors hearts ($n = 5$) and failing human IHD hearts ($n = 6$ hearts per experimental group; $^*P < 0.05$ vs. normal donor hearts). **c** Real-time PCR analyses of CARD3 mRNA levels in samples from wild-type (WT) control mice after sham or MI surgery at the indicated time points ($n = 4$ mice per experimental group, $^*P < 0.05$ vs. shams). **d** Representative western blots of CARD3 protein levels in an experimental mouse MI model at the indicated times ($n = 4$ mice per experimental group; $^*P < 0.05$ vs. shams). *Top* representative blots. *Bottom*, quantitative results. The data are presented as the mean ± SEM and are representative of at least three independent experiments

pathological processes post-MI. To further investigate the potential involvement of CARD3 in vivo, a mouse model with a global knockout of CARD3 (CARD3-KO) was utilised and examined at 4 weeks after the sham or MI operation (Fig. 2a). At baseline, CARD3-KO mice manifested no pathological abnormalities with respect to cardiac structure or function. In addition, all of the sham-operated mice survived surgery and to the end of the observation period (100 vs. 100 %, respectively). However, only 16 (50.0 %) of 32 WT littermate controls mice and 21 (61.8 %) of 34 CARD3-KO survived until 28 days after MI ($P < 0.05$; Fig. 2b). Kaplan–Meier curves revealed that the highest mortality occurred during the first week after MI (Fig. 2b), indicating a selective detrimental effect of CARD3 at this stage. More specifically, at autopsy, we found that 68.6 % of the non-surviving WT mice (11/16) died of cardiac rupture, while 53.8 % of the non-surviving CARD3-KO mice (7/13) died of cardiac rupture ($P < 0.05$; data not shown); these findings demonstrate that cardiac rupture may be the major cause of death. In line with the decreased mortality, H&E staining at 4 weeks after MI further displayed a significantly constricted infarct size in CARD3-KO mice compared with WT control animals ($P < 0.05$; Fig. 2c, d). Consistently with our observations at 4 W post-MI, infarct size were significantly reduced in CARD3-KO mice, compared with their controls at 3 days

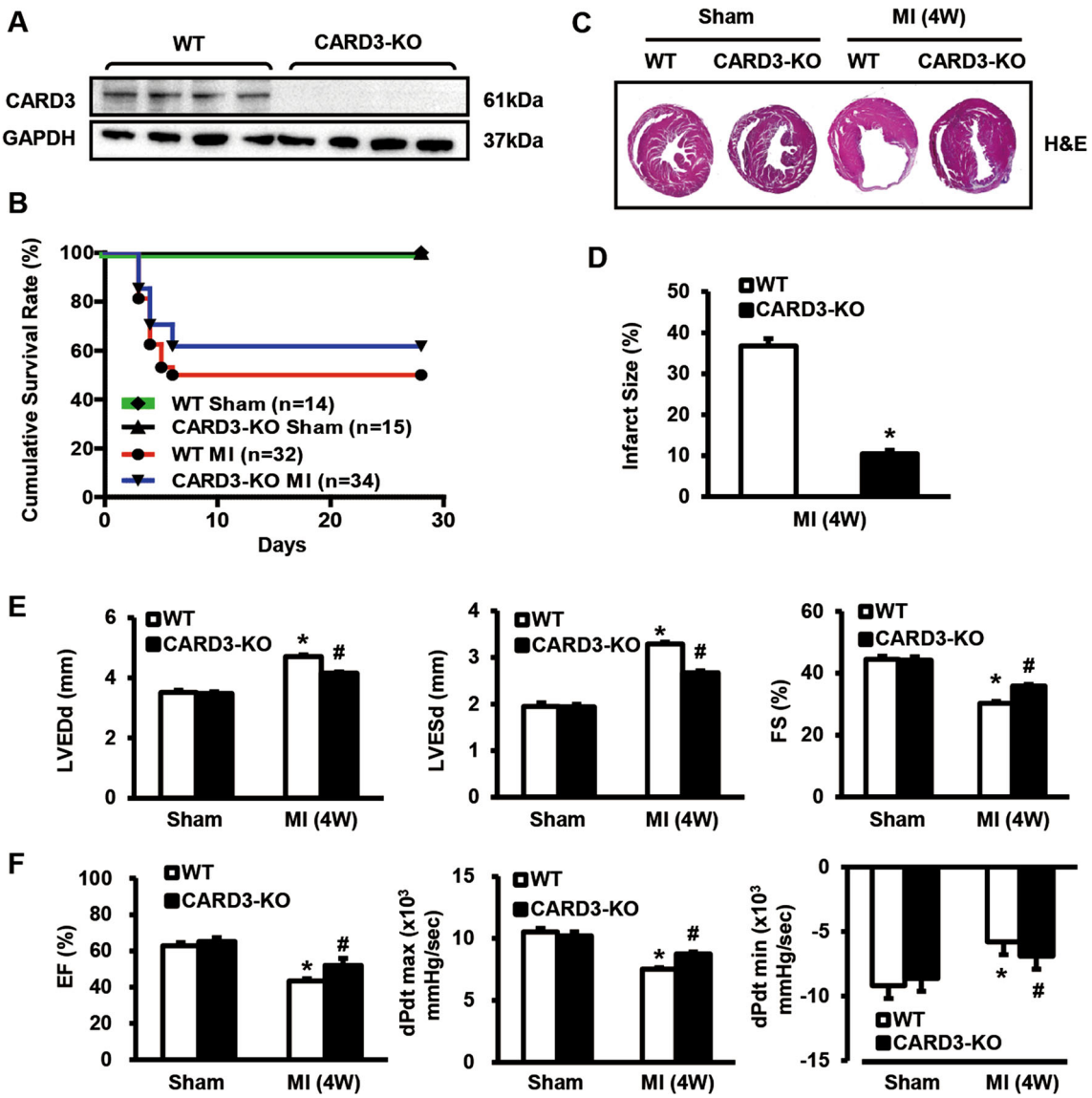

Fig. 2 Loss of CARD3 promotes survival rates, reduces infarct size, and improves cardiac function after MI. **a** Representative western blots of CARD3 expression in heart tissues from wild-type (WT) littermates and CARD3-knockout (CARD3-KO) mice ($n = 4$ mice per experimental group). **b** Kaplan–Meier survival curves from WT and CARD3-KO mice subjected to sham or MI operation. **c** Histological analysis of hematoxylin and eosin (H&E)-stained WT and CARD3-KO hearts at 4 weeks after MI ($n = 6$–8 mice per experimental group). **d** Statistical results for relative infarct size (%) in the indicated groups ($^*P < 0.05$ vs. WT/MI). **e**, **f** Measurements of echocardiographic and haemodynamic parameters (LVEDD, LVESD, FS %, EF %, dP/dt_{min}, and dP/dt_{max}) in the indicated groups at 4 weeks after MI ($n = 8$–12 mice per experimental group; $^*P < 0.05$ vs. WT/sham; $^{\#}P < 0.05$ vs. WT/MI)

after MI (Supplemental Fig. S4a). Moreover, cardiac function was assessed with serial echocardiography on week 4 post-MI. We observed that while LV end-diastolic dimension (LVEDd) and LV end-systolic dimension (LVESd) were lower and fractional shortening percentage (FS %) was higher in both WT and CARD3-KO infarcted mice. CARD3-KO mice exhibited more attenuated systolic function and restrained LV dilatation than WT mice (Fig. 3e). Accordingly, haemodynamic measurements further revealed increased LV contraction in CARD3-null mice, as measured by ejection fraction percentage (EF %), dP/dt_{max}, and dP/dt_{min} (Fig. 3f). Overall, these data provide supporting evidence that the absence of CARD3 in the heart not only reduces mortality but also inhibits infarct expansion and functional deterioration following MI.

Cardiac-specific overexpression of CARD3 increases MI-induced mortality, exacerbates infarct size expansion, and promotes cardiac dysfunction

To specifically define the effects of CARD3 on the heart, we next sought to determine whether overexpression of

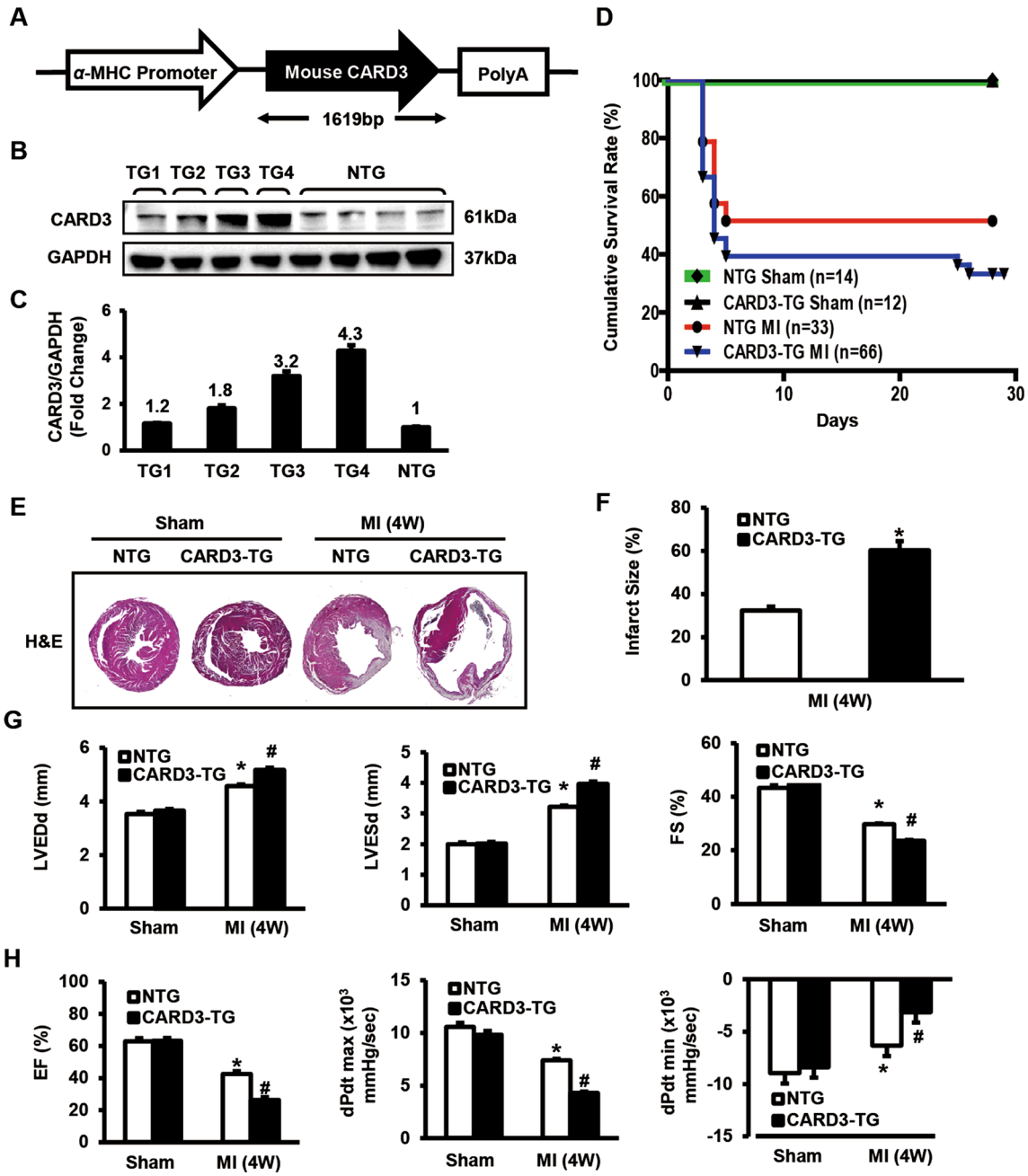

Fig. 3 Overexpression of CARD3 increases mortality and exacerbates infarct size expansion, as well as heart functional deterioration following MI. **a** Schematic diagram of the construction of transgenic (TG) mice with full-length mouse CARD3 cDNA under the control of the α-myosin heavy chain (α-MHC) promoter. **b** Representative western blots for the determination of CARD3 protein expression in heart tissues from 4 lines of TG mice and their non-transgenic (NTG) littermates ($n = 4$ mice per experimental group). **c** Quantitation of CARD3 expression in heart tissues from 4 TG and NTG mouse lines. **d** Kaplan–Meier survival curves of NTG and CARD3-TG mice at 4 weeks after sham or MI surgery. **e** H&E staining in NTG and CARD3-TG mice at 4 weeks post-MI ($n = 5$–7 mice per experimental group). **f** Relative infract size (%) in the indicated groups ($^*P < 0.05$ vs. NTG/MI). **g, h** Parameters of the echocardiographic and haemodynamic results (LVEDD, LVESD, FS %, EF %, dP/dt_{min}, and dP/dt_{max}) for NTG and CARD3-TG mice following MI ($n = 9$–11 mice per experimental group; $^*P < 0.05$ vs. NTG/sham; $^{\#}P < 0.05$ vs. NTG/MI)

CARD3 could affect myocardium in the setting of MI. To this end, we generated inducible, cardiac-specific transgenic (TG) mice expressing mouse CARD3 using the α-MHC promoter (Fig. 3a). Four germ lines of CARD3-TG mice were verified by western blot analysis (Fig. 3b). Under basal conditions, all of the CARD3-TG mice were healthy and displayed no apparent cardiac morphological or pathological abnormalities. We then selected transgenic

line 4 (Fig. 3c), which expressed the highest levels of CARD3, for further experiments. CARD3-TG mice and their non-transgenic littermates (referred to as NTG) were subjected to MI surgery or a sham operation and examined after 4 weeks. The survival rate up to 4 weeks after MI was significantly lower in CARD3-TG mice than in NTG mice. As depicted in Fig. 3d, 17 out of 33 male NTG mice (51.5 %) survived to 28 days post-MI. In contrast, 22 out of 66 CARD3-TG mice (33.3 %) survived to 28 days following MI ($P < 0.05$). The main cause of death was attributable to cardiac rupture, the incidence of which was significantly higher in CARD3-TG mice than in NTG mice (data not shown). Similarly, by 28 days post-MI, morphometric analyses exhibited a 28.0 % greater infarct size in CARD3-TG mice compared with NTG control mice (Fig. 3e, f). Consistently with our observations at 4 W post-MI, infarct size were dramatically increased in CARD3-TG mice compared with their controls at 3 days after MI (Supplemental Fig. S4b). Furthermore, echocardiographic and haemodynamic analyses revealed more pronounced LV dilatation and more severe contractile dysfunction in TG than in NTG infarcted hearts 28 days post-MI, as determined by LVEDd, LVESd, FS %, EF %, dP/dt_{max}, and dP/dt_{min} (Fig. 3g, h). Together, these results indicate that CARD3 overexpression aggravated post-infarction mortality, infarct size enlargement, and cardiac dysfunction.

CARD3 activation facilitates MI-induced cardiomyocyte apoptosis

Apoptosis has been proposed as an important mechanism for the elimination of cardiomyocytes after MI [4]. Therefore, we evaluated the direct effect of overexpressed or knockdown CARD3 on cardiomyocyte apoptosis in our animal model. To detect apoptosis, myocardial tissue sections in the infarct border zone were stained with TUNEL staining. Notably, in sham-operated hearts, TUNEL-positive nuclei were rarely observed. However, in response to MI, the number of TUNEL-positive nuclei was increased in NTG hearts and very clearly increased in CARD3-TG hearts ($\approx$38.6 % TUNEL-positive nuclei, $P < 0.05$; Fig. 4c, d). In contrast, CARD3-KO hearts exhibited significantly less TUNEL-positive nuclei ($\approx$20.6 % TUNEL-positive nuclei, $P < 0.05$; Fig. 4a, b). Meanwhile, apoptotic cardiomyocytes were significantly reduced in CARD3-KO mice, but dramatically increased in CARD3-TG mice compared with their controls, respectively, at 3 days after MI (Supplemental Fig. S4c-d), suggesting that the inhibition of endogenous CARD3 in the heart could impair myocyte apoptosis following MI. To clarify the pro-apoptotic effect of CARD3 in vivo, we first examined the expression of apoptosis-related genes, including Bcl-2, Bid, Bak, and cleaved caspase 3. Real-time PCR revealed that CARD3-null hearts clearly promoted the MI-induced expression of the anti-apoptotic protein Bcl-2 induced by MI (Fig. 4e), whereas the overexpression of CARD3 resulted in a significant down-regulation of Bcl-2 in response to MI (Fig. 4f). Additionally, western blot analyses displayed that CARD3 expression preserved the expression of the pro-apoptotic proteins Bid, Bak, and cleaved (active) caspase-3 at 28 days post-MI (Fig. 4g, h). Thus, the above results in vivo suggest that CARD3 may be an important modulator of the apoptotic cascade upon MI.

Because apoptosis was increased in the CARD3-TG hearts and reduced in the CARD3-KO hearts in the MI model, we sought to determine whether CARD3 in cultured neonatal rat cardiomyocytes (NRCMs) influences cellular tolerance to hypoxia injury in vitro. Primary cultured cardiomyocytes were infected with either AdCARD3 (adenoviral CARD3) to overexpress CARD3 or AdshCARD3 (adenoviral short hairpin CARD3) to knockdown CARD3 and subsequently exposed to hypoxia for 48 h (Fig. 4i). In line with the in vivo results, our in vitro data showed that loss of CARD3 blocked the apoptotic effects of hypoxia (Fig. 4j, k), as indicated by more PI-stained cells. In contrast, the overexpression of CARD3 promoted hypoxia-induced apoptosis (Fig. 4l, m), compared with the controls. In addition, these findings were supported by the LDH (lactate dehydrogenase; cell toxicity) and CCK8 (cell counting kit-8; cells viability) assays, as CARD3 expression significantly promoted greater LDH release and suppressed CCK8 expression in response to hypoxia (Fig. 4n, o). Accordingly, the ratio of protein/DNA and the expression of pro-apoptotic markers (Bid, Bax, and cleaved caspase-3) were profoundly suppressed in AdshCARD3-infected cardiomyocytes (Fig. 4p). In comparision, these measurements were remarkably aggravated in AdCARD3-infected cells, compared with the controls, respectively (Fig. 4q). These ex vivo data are consistent with the aforementioned data from the in vivo MI model and demonstrate that CARD3 promotes cardiomyocyte apoptosis, at least in part, through the regulation of apoptosis-related gene expression.

CARD3 enhances inflammatory response following MI

Given that inflammation is believed to be a crucial determinant for the myocardial healing process [35] and that CARD3 has been shown to be a modulator of inflammation [55], we further determined whether expression of CARD3 could influence the inflammatory response in the peri-infarct areas. The number of CD3 (labels lymphocytes), Ly6G (neutrophils), and Mac-1 (monocytes/macrophages) positive cells were analysed by immunofluorescent

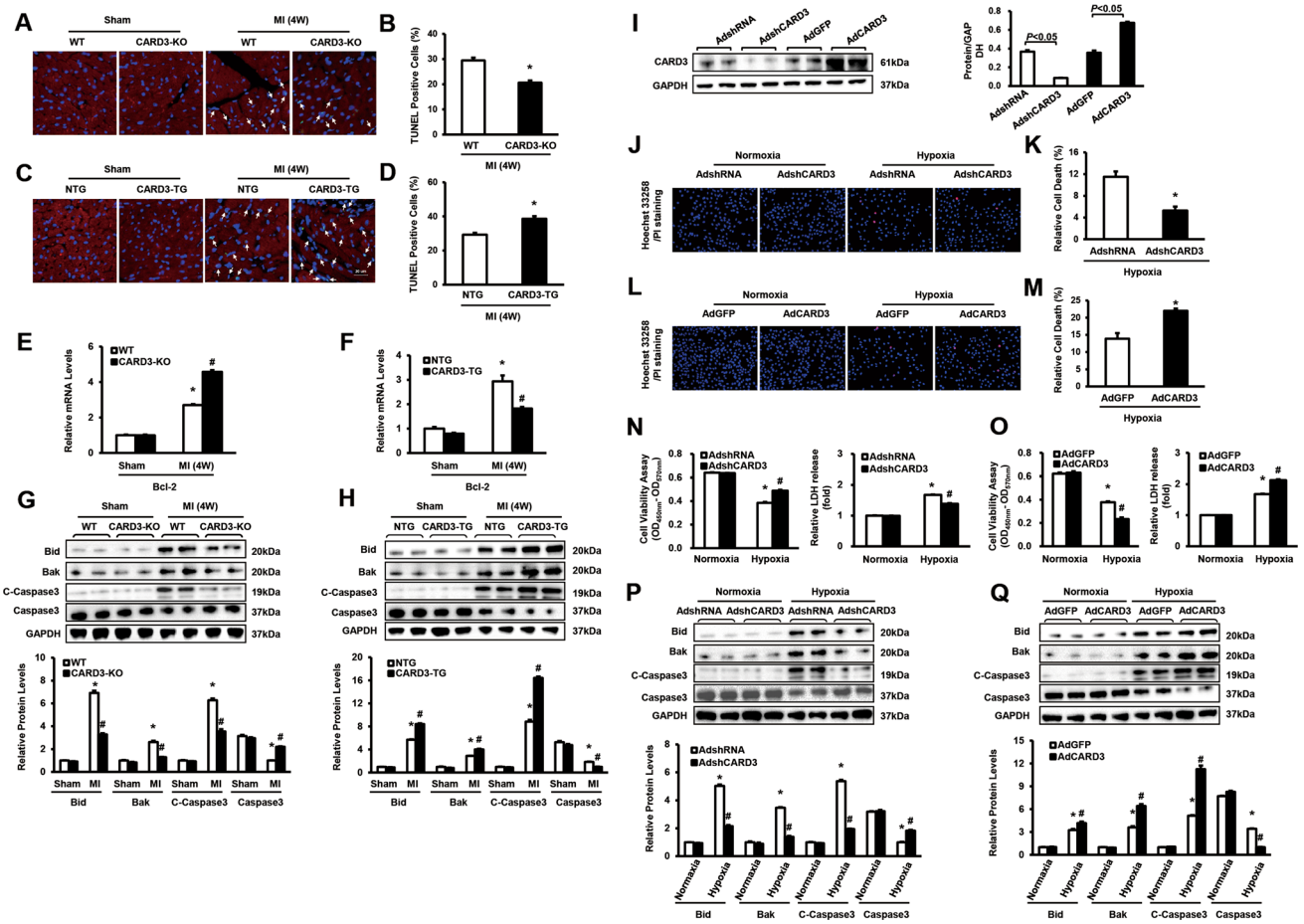

Fig. 4 CARD3 activation facilitates cardiomyocyte apoptosis and regulates genes involved in apoptosis in response to MI. **a** Representative merged images showing cardiomyocyte apoptosis in the border zone of WT and CARD3-KO hearts at 4 weeks post-MI ($n = 4$ mice per experimental group; magnification, 400×). Apoptotic cells from the border zone were labelled via TUNEL (terminal deoxynucleotidyl-transferase-mediated dUTP nick-end labelling) staining (*green*). α-Actinin, a myocyte-specific marker (*red*), was used to visualise cardiomyocytes and DAPI (4,6-diamidino-2-phenylindole; *blue*) was applied to label nuclei. **b** The quantification of rates of apoptosis is expressed as a percentage of total cells counted ($n = 500 +$ nuclei per experimental group; $^{*}P < 0.05$ vs. WT/MI). **c** TUNEL staining in the border zone of NTG and CARD3-TG hearts at 4 weeks post-MI ($n = 4$ mice per experimental group). **d** The quantitative results of apoptotic rates ($n = 500 +$ nuclei per experimental group; $^{*}P < 0.05$ vs. NTG/MI). **e**, **f** Real-time PCR analysis of Bcl-2 in the peri-infarct areas of (**e**) WT and CARD3-KO mice and (**f**) NTG and TG mice at 4 weeks after sham or MI surgery ($n = 4$ mice per experimental group, $^{*}P < 0.05$ vs. WT or NTG/sham; $^{\#}P < 0.05$ vs. WT or NTG/MI). **g**, **h** Representative western blots and quantitative results of Bid, Bak, and cleaved caspase 3 in (**g**) WT and CARD3-KO mice and (**h**) NTG and CARD3-TG mice at 4 weeks post-MI ($n = 4$ mice per experimental group, $^{*}P < 0.05$ vs. WT or NTG/sham; $^{\#}P < 0.05$ vs. WT or NTG/MI). **i** The protein expression level of CARD3 after infection with AdshCARD3, AdCARD3, or their respective controls (AdshRNA and AdGFP) was analysed by western blotting ($n = 4$ independent experiments). *Left* representative blots. *Right* quantitative results. **j**, **l** Representative merged images of NRCMs infected with (**j**) AdshCARD3 or (**l**) AdCARD3 adenoviral vector-infected cardiomyocytes treated with hypoxia for 48 h ($n = 3$ independent experiments; magnification, 400×). Nuclei (Hoechst 33258, *blue*), positive staining (*red*). **k**, **m** The quantification of rates of apoptosis ($n = 200 +$ nuclei per experimental group; $^{*}P < 0.05$ vs. WT or NTG/MI). **n**, **o** LDH (lactate dehydrogenase; cell toxicity) and CCK8 (cell counting kit-8; cells viability) assay detected in (**n**) CARD3-knockdown or (**o**) CARD3-overexpressing cells after hypoxia for 48 h ($n = 3$ independent experiments; $^{*}P < 0.05$ vs. AdshRNA or AdGFP/normoxia; $^{\#}P < 0.05$ vs. AdshRNA or AdGFP/hypoxia). **p**, **q** Representative western blots and quantitative results of Bid, Bak, and cleaved caspase 3 in (**p**) AdshCARD3 or (**q**) AdCARD3 after hypoxia for 48 h ($n = 4$ independent experiments, $^{*}P < 0.05$ vs. AdshRNA or AdGFP/normoxia; $^{\#}P < 0.05$ vs. AdshRNA or AdGFP/hypoxia). *Top* representative blots. *Bottom* quantitative results

staining. Interestingly, the numbers of CD3, Ly6G, and Mac-1 positive cells were clearly decreased in the hearts of CARD3-KO compared with WT hearts subjected to MI for 7 days (Fig. 5a, b). In contrast, CARD3-TG hearts after MI exhibited significantly higher numbers of neutrophils, monocytes/macrophages, and lymphocytes in comparison with NTG-MI hearts (Fig. 5c, d). Accordingly, the mRNA levels of several inflammatory markers, including IL-1β (interleukin 1β) and monocyte chemotactic protein 1 (MCP-1) were much lower in CARD3-KO mice than in

WT mice 7 days after MI (Fig. 5e). However, the expression of these cytokines was significantly amplified in CARD3-TG mice (Fig. 5f). The above results indicate that the degrees of inflammatory cell infiltration and cytokines release were greatly enhanced by the presence of CARD3.

More importantly, abundant evidences have demonstrated that the induction of these inflammatory-related genes involves the activation of canonical NF-κB pathway [26]. Therefore, we next monitored the activation of NF-κB. We clearly detected IκBα phosphorylation and IκBα degradation 7 days post-MI in WT mice (Fig. 5g). However, IκBα phosphorylation and IκBα degradation were significantly impaired in CARD-KO mice (Fig. 5g). Conversely, after 7 days post-MI, the CARD3-TG mouse hearts consistently exhibited increased the phosphorylation and degradation of IκBα, compared with NTG (Fig. 5h). Notably, the phosphorylation of P65 is essential for NF-κB activation [50]. We also tested the effect of CARD3 on MI-induced phosphorylation of P65. As showed in Fig. 5g, MI-induced the phosphorylation of P65 as determined by western blot analysis 7 days after MI were abrogated in CARD3-KO mice. In contrast, this phosphorylation was strengthened in CARD3-TG mice (Fig. 5h). Collectively, these data suggest that the CARD3-mediated inflammatory response post-MI may be partly attributable to the activation of NF-κB cascades.

CARD3 modulates maladaptive LV remodelling in response to MI

Importantly, cardiomyocyte loss and the resultant increase in haemodynamic overload triggers an adaptive hypertrophy [31]. We therefore further examined the effects of CARD3 on hypertrophic response post-MI. As showed in Fig. 6a–c, the hearts of CARD3-KO mice exhibited significantly attenuated cardiac hypertrophy 4 weeks after MI compared with WT littermates, as evidenced by a decreased heart weight (HW)/body weight (BW) ratio, HW/tibia length ratio, lung weight (LW)/BW ratio, and cardiomyocyte cross-sectional area (CSA). However, in response to MI-triggered cell hypertrophy, CARD3-TG mice exhibited remarkably increased myocyte hypertrophy (Fig. 6g–i). Consistent with these morphological alterations, the expression levels of several hypertrophic markers [including atrial natriuretic peptide (ANP), brain natriuretic peptide (BNP), and β-myosin heavy chain (β-MHC)] in the infarcted hearts were significantly down-regulated during CARD3 knockdown (Fig. 6e) and up-regulated during CARD3 overexpression (data not shown).

To further define the effects of CARD3 on post-infarction cardiac remodelling, we determined the extent of reactive fibrosis induced by MI. Heart sections were stained with picrosirius red (PSR) to detect fibrosis. Our results revealed that interstitial fibrosis spaces and collagen volumes were noticeably limited in CARD3-KO hearts (Fig. 6b, d) subjected to MI but were dramatically exaggerated in CARD3-TG hearts (Fig. 6h, j). Analysis of the mRNA levels of mediators of fibrosis, including connective tissue growth factor (CTGF), collagen I, and collagen III were consistently greatly suppressed in CARD3-KO mice (Fig. 6f). In contrast to CARD3 deficiency, CARD3 overexpression remarkably enhanced MI-induced cardiac fibrosis compared with controls (data not shown). Taken together, these data imply that the presence of CARD3 in the heart contributes to adverse post-infarction LV remodelling.

CARD3 mediates post-MI cardiac remodelling via the activation of p38 pathways

The above results indicated that CARD3 may play a detrimental role on cardiac remodelling after MI. However, the underlying molecular mechanisms by which CARD3 exert its adverse effects on post-infarction remodelling remains unclear. The modulation of the MAPK signalling cascade may contribute to the myocardial response to ischemic injury and regulate cellular events critical for post-MI LV remodelling [1]. Therefore, we sought to investigate whether CARD3 interferes with MAPK cascade activation upon MI. Unexpectedly, following MI, neither overexpression nor ablation of CARD3 in mouse hearts changed the expression level of phosphorylated MEK1/2, ERK1/2, and JNK1/2 (Fig. 7a, b). However, CARD3-TG mice exhibited higher levels of phosphorylated p38 in response to MI compared with those of NTG mice (Fig. 7b). More importantly, MI-triggered activation of p38 was almost completely abrogated in CARD3-KO hearts compared with WT controls (Fig. 7a). To further confirm the positive correlation between CARD3 and p38 expression in the in vitro paradigm, cultured NRCMs were exposed to hypoxia after infection with AdCARD3 to overexpress CARD3 or AdshCARD3 to knockdown CARD3. Similar to the in vivo observations, the levels of p38 were reduced in the AdshCARD3 cells compared with the control AdshRNA cells (Fig. 7c). In contrast, the overexpression of CARD3 enhanced levels of p38 compared with those observed in the control cells (Fig. 7d). These findings indicate that those activation of p38 pathway was responsible for the CARD3-elicited deteriorative effects on cardiac remodelling after MI.

Discussion

Herein, we have identified CARD3 as an intrinsic positive regulator of maladaptive post-infarction remodelling and transition to heart failure. The major novel findings of this

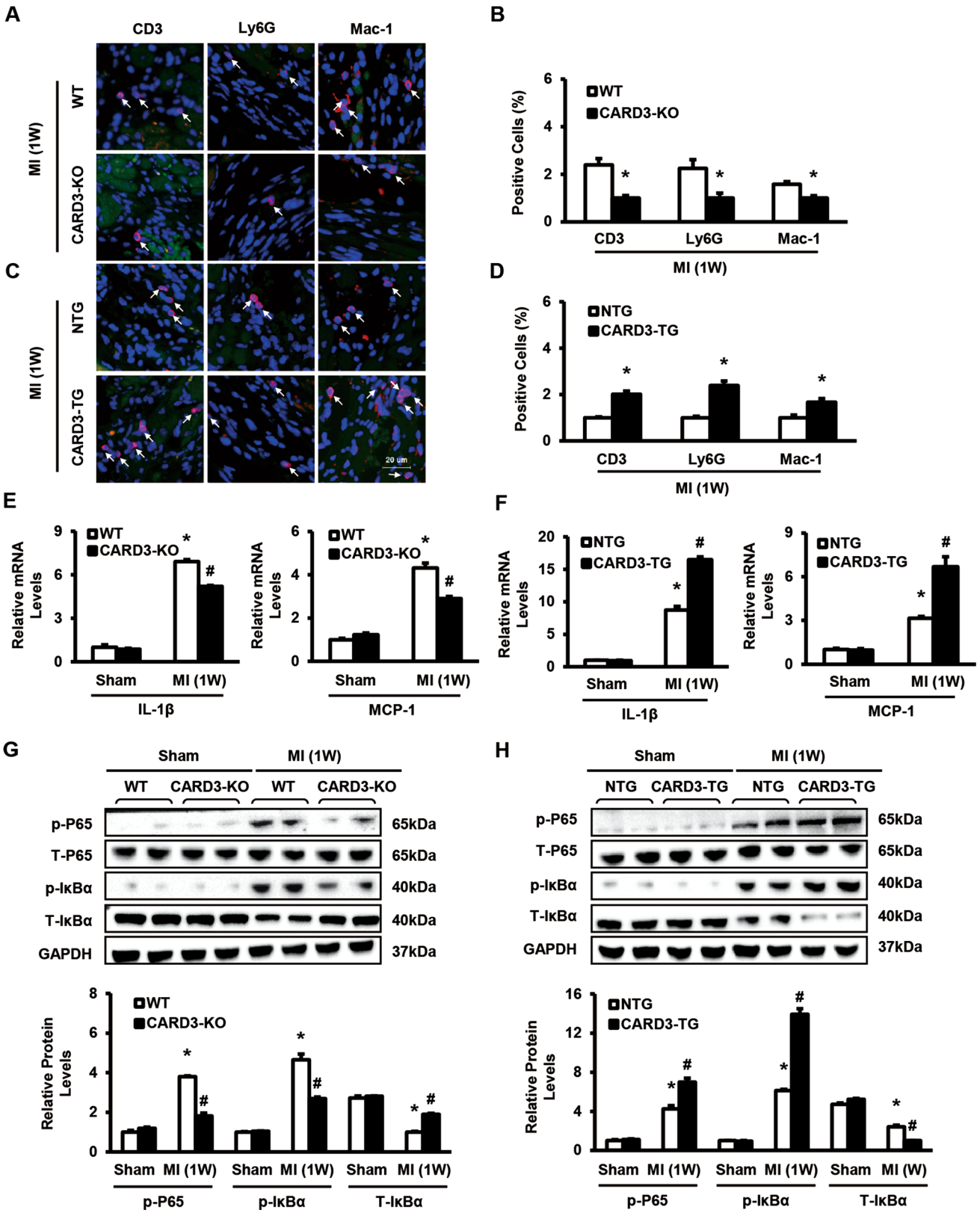
A
CD3
Ly6G
Mac-1
MI (1W)
WT
CARD3-KO
20 um
B
Positive Cells (%)
WT
CARD3-KO
CD3
Ly6G
Mac-1
MI (1W)
C
MI (1W)
NTG
CARD3-TG
D
Positive Cells (%)
NTG
CARD3-TG
E
Relative mRNA Levels
WT
CARD3-KO
Sham
MI (1W)
IL-1β
MCP-1
F
Relative mRNA Levels
NTG
CARD3-TG
G
Sham
MI (1W)
WT
CARD3-KO
p-P65
T-P65
p-IκBα
T-IκBα
GAPDH
65kDa
40kDa
37kDa
Relative Protein Levels
p-P65
p-IκBα
T-IκBα
H
NTG
CARD3-TG

◀**Fig. 5** CARD3 enhances detrimental inflammatory responses after MI. **a**, **c** Immunofluorescent staining showing the number of CD3-, Ly6G-, and Mac-1-positive cells in the border zone of (**a**) WT and CARD3-KO mice and (**c**) NTG and TG mice at 1 week post-MI ($n = 3$ independent experiments;). **b**, **d** The quantitative analysis of positive cells in the border zone of (**b**) WT and CARD3-KO hearts and (**c**) NTG and CARD3-TG hearts post-MI ($^*P < 0.05$ vs. WT or NTG/MI). **e**, **f** Real-time PCR assays of IL-1β and MCP-1 in hearts from (**e**) WT and CARD3-KO mice and (**f**) NTG and CARD3-TG mice at 1 week after sham or MI operation ($n = 4$ mice per experimental group, $^*P < 0.05$ vs. WT or NTG/sham; $^{\#}P < 0.05$ vs. WT or NTG/MI). **g**, **h** Representative blots and quantitative results of the P65 and IκBα in (**g**) WT and CARD3-KO mice and (**h**) NTG and CARD3-TG mice after treatment with MI for 1 week ($n = 4$ mice per experimental group, $^*P < 0.05$ vs. WT or NTG/sham; $\#P < 0.05$ vs. WT or NTG/MI). *Top* representative blots. *Bottom* quantitative results

study are as follows: (1) CARD3 expression was significantly up-regulated in both human IHD hearts and mouse post-infarction hearts; (2) the MI-induced disruption of CARD3 in the heart respond to MI resulted in cardioprotection in terms of reduced mortality and infarct size, and improved LV functional deterioration. Strikingly, this protective effect in CARD3-nulled hearts is associated with decreased cardiomyocyte apoptosis, blunted inflammatory response, as well as impaired LV remodelling. However, the overexpression of CARD3 in hearts subjected to MI obviously aggravated these pathological processes post-MI; (3) CARD3-mediated post-infarction remodelling was largely dependent on the activation of the NF-κB and p38 signalling pathways; (4) parallel in vitro experiments confirmed these in vivo observations. Collectively, we have provided evidence that CARD3 plays a critical role in the development of MI and revealed that targeting CARD3 could be a potential therapeutic strategy for preventing maladaptive remodelling following MI.

Accumulating evidences has demonstrated that a sudden increase in cardiomyocyte apoptosis occurs in the ischemic hearts of both patient and animals [14, 40], and apoptosis leads to continuous cardiomyocyte loss throughout the entire pathological process post-MI [4]. Moreover, inhibition of cardiomyocyte apoptosis has shown potential protection against post-MI cardiac dysfunction and remodelling [2]. The experimental findings herein show a correlation between an increase in the frequency of apoptosis and the extent of infarct size. Accordingly, we observed that reduced cardiac myocyte apoptosis contributed significantly to markedly decreased infarct size in CARD3-KO mice compared with infarcts in WT control mice. In contrast, the overexpression of CARD3 significantly enhances MI-induced myocyte death and infarct size in response to MI. However, previous reports indeed have showed that CARD3 does not influence infarct size after myocardial ischemic injury induced by ischemia–reperfusion but not permanent occlusion (used in our study). In their study, all the mice underwent 30 min of global ischemia followed by 120 min of reperfusion; this is an acute MI model to study ischemia–reperfusion injury which mimics the injury induced by coronary recanalization or heart transplantation. However, in our present study, the permanent occlusion was used to establish the MI model, in which the main pathological changes were cell death, cardiac remodelling (*e.g.,* cardiac hypertrophy and fibrosis). Our results showed that in the early stage (3 h), neither CARD3-KO nor CARD3-TG affects infarct size indicated by Evens blue staining (Supplemental Figure S1), which is consistent with Sicard's and Jacquet's studies [19, 45]. However, observing from our experiment, CARD3 exhibits deteriorated function against heart damage as early as 3 days after MI via promoting cardiomyocytes apoptosis. Importantly, our investigations also suggested that apoptotic cardiomyocyte loss early after ischemic injury indeed contributes to cardiac remodeling and failure. After 4 weeks of MI, numerous of cardiac cell death are responsible for infarct size enlargement in the WT mice and NTG mice, and CARD3 deficiency significantly inhibits MI-induced cell death and infarct size enlargement, whereas CARD3 overexpression remarkably aggravate these processes. Thus, Sicard's and Jacquet's studies and our results were mutually complementary rather than exclusive. In support of our observations, previous studies have suggested that in other cell lines, such as the MCF7 breast cancer cells and human embryonic kidney cells, the overexpression of CARD3 also leads to enhanced apoptosis [32]. Moreover, mutational analysis revealed that the CARD domain is both sufficient and necessary for CARD3-mediated apoptosis [32]. Thus, CARD3 may serve as a positive regulator for apoptosis after MI. Importantly, our observation of an increase in the number of apoptotic cells in the myocardium of CARD3-TG mice support the hypothesis that cardiomyocytes die, in part through an apoptotic pathway, following acute MI. Furthermore, it has been demonstrated that cardiomyocytes have a very large energy requirement and contain the highest density of mitochondria of all mammalian cells [39]. In healthy cells, their primary function is providing ATP through oxidative phosphorylation. However, under stress signals, including hypoxia, oxidative stress and DNA damage, mitochondria acts as central regulators of apoptosis [12]. Severe ischemia during MI can promote permeabilization of the mitochondrial outer membrane, causing the release of pro-apoptotic signalling molecules, such as cytochrome c, apoptotic protease-activating factor 1, and endonuclease G, thereby activating the apoptotic pathway [4]. Moreover, the permeability of mitochondrial membrane is strictly regulated by a family of proteins known as the Bcl-2 family, including Bcl-2, Bax, Bid, Bak, etc. [57]. Indeed, our in vivo and in vitro data revealed that the presence of

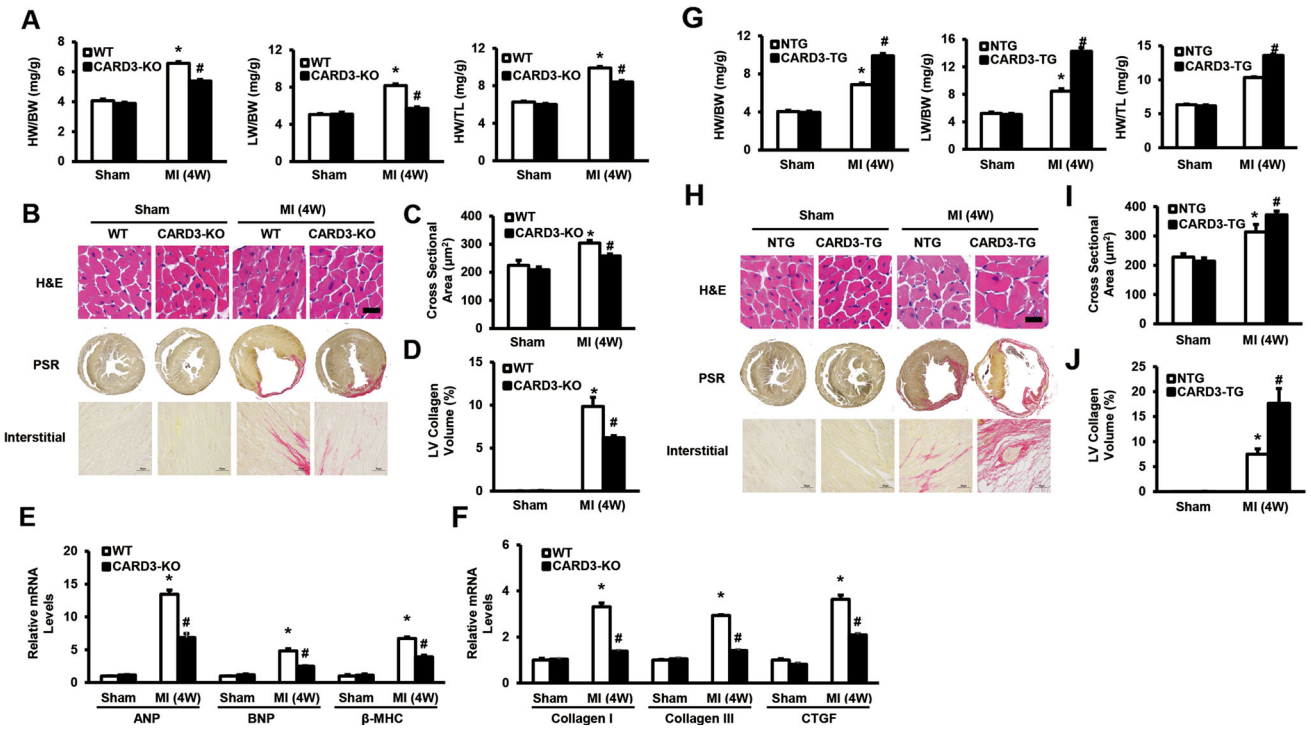

Fig. 6 CARD3 mediates maladaptive cardiac remodelling following MI. **a** The HW/BW, LW/BW, and HW/TL ratios determined in WT and CARD3-KO mice after sham or MI treatment ($n = 8$–11 mice per experimental group). **b** Histological analysis using H&E and PSR staining in WT and CARD3-KO mice at 4 weeks after MI surgery ($n = 5$–8 mice per experimental group, *scale bars* 20 μm for H&E staining, *scale bars* 50 μm for PSR staining). **c** The statistical results for the ratios of cross-sectional area (CSA, $n = 100 +$ cells per experimental group). **d** Statistical results for LV collagen volume (%) ($n = 25 +$ fields per experimental group). **e** Real-time PCR analyses of the hypertrophic markers ANP, BNP, and β-MHC induced by MI in WT and CARD3-KO mice ($n = 4$ mice per experimental group). **f** Real-time PCR analyses of fibrotic markers (collagen I, collagen III, and CTGF) in the indicated groups ($n = 4$ mice per experimental group). **g** The ratios of HW/BW, LW/BW, and HW/TL ($n = 8$–10 mice per experimental group) in the NTG and CARD3-TG mice at 4 weeks after sham or MI surgery. **h** Histological analyses of the H&E and PSR staining of the indicated groups at 4 weeks after MI surgery ($n = 5$–7 mice per experimental group; *scale bar* 20 mm for H&E staining, *scale bar* 50 mm for PSR staining). **i**, **j** Statistical results for the ratios of (**i**) CSA ($n = 100 +$ cells per experimental group); (**j**) LV collagen volume ($n = 25 +$ fields per experimental group). $^{*}P < 0.05$ versus WT or NTG/sham; $^{\#}P < 0.05$ versus WT or NTG/MI

CARD3 in the hearts significantly enhanced the activation of terminal effector caspase, cleaved caspase-3, and indicated that cardiomyocyte apoptosis in post-MI hearts is associated with decreased Bcl-2 level and increased Bak and Bid levels. Thus, CARD3-mediated apoptosis in cardiomyocytes may occur primarily via the mitochondrial apoptosis pathway.

It has been well documented that innate immune and inflammatory responses are involved in the pathophysiological processes of myocardial ischaemic injury [8, 47]. Cardiomyocyte death results in marked induction of chemokines and cytokines in the infarcted myocardium, where they recruit and activate neutrophils and mononuclear cells [35]. During the inflammatory phase, infiltration by inflammatory cells, particularly neutrophils and macrophages, is followed by degradation of extracellular matrix constituents and the scavenging of dead cardiac myocytes and their debris [10]. Indeed, we discovered remarkable neutrophil, macrophage, and lymphocytes infiltration in the infarcted hearts at 7 days after MI, with these cells constituting the acute post-MI inflammatory response after MI. Consistent with their central role in triggering inflammation, the levels of pro-inflammatory cytokines, such as IL-1β and MCP-1, were also obviously increased in TG-MI mice but reduced in KO-MI mice, compared with their respective counterparts. These results indicate that myocyte CARD3 activation was essential for the inflammatory response in the infarcted heart. Moreover, the activation of NF-κB is thought to be a strong inducer of the expression of these pro-inflammatory cytokines [48], and activated NF-κB has been detected in post-MI remodelling [36]. In this regard, our experimental finding further showed that CARD3 promotes NF-κB signalling by regulating IκBα phosphorylation and degradation. Such findings are consistent with a previous study that CARD3 induces IKKγ/NEMO ubiquitinylation, thereby controlling NF-κB activation [17]. Moreover, Levin et al. [23] demonstrated that CARD3 deficiency prevented local and

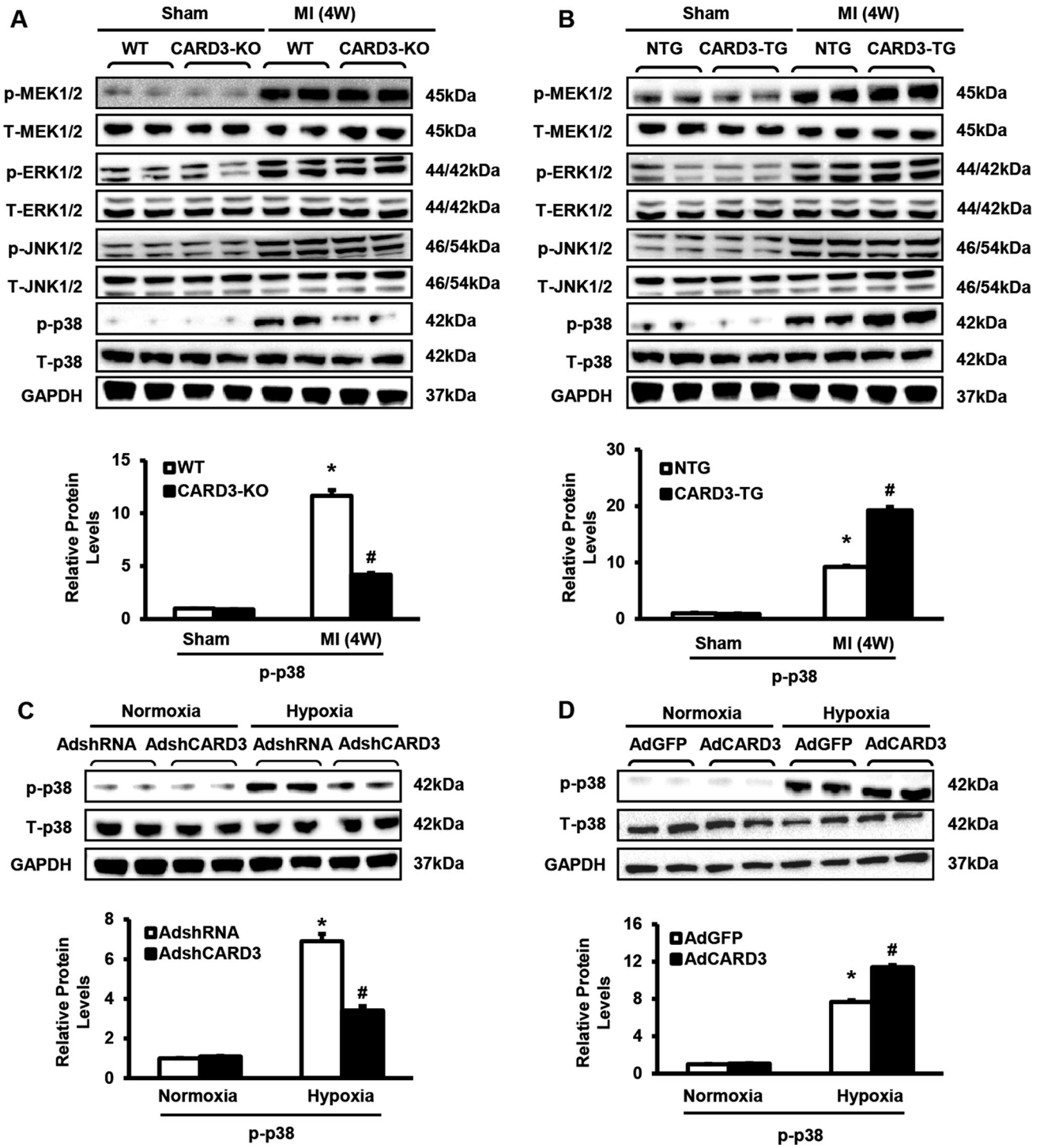

Fig. 7 CARD3 modulates post-MI cardiac remodelling through the activation of p38 pathways. **a**, **b** Representative western blots and quantitative results showing the phosphorylation and total protein levels of MEK1/2, ERK1/2, JNK1/2, and p38 in (**a**) WT and CARD3-KO mice and (**b**) NTG and TG mice subjected to MI or sham surgery after 4 weeks ($n = 5$ mice per experimental group, $^{*}P < 0.05$ vs. WT or NTG/sham; $^{\#}P < 0.05$ vs. WT or NTG/MI). **c**, **d** Representative western blots of p38 in (**c**) AdshCARD3 or (**d**) AdCARD3 after normoxia or hypoxia for 48 h ($n = 4$ independent experiments, $^{*}P < 0.05$ vs. AdshRNA or AdGFP/normoxia; $^{\#}P < 0.05$ vs. AdshRNA or AdGFP/hypoxia). *Top* representative blots. *Bottom* quantitative results

systemic inflammation in atherosclerosis. More importantly, it was recently demonstrated that the regulation of CARD3 involves a novel feed-forward regulatory mechanism. Specifically, CARD3 positively regulates NF-κB activity, and the inflammatory cytokines that activate the NF-κB pathway induce increased CARD3 expression

[55]. Thus, our results suggest that CARD3 expression is involved in the activation of NF-κB, resulting in exacerbation of the inflammatory response and subsequent myocardial damage post-MI.

Adverse LV remodelling is known to contribute to morbidity and mortality after MI. This process includes a combination of concentric and eccentric hypertrophy, cardiac fibrosis, and subsequent LV dysfunction, leading to heart failure [37]. Indeed, myocyte death within the infarcted and non-infarcted myocardium plays an intricate role not only in the infarction expansion and thinning but also in cell slippage in the non-infarcted myocardium. These effects permit longitudinal hypertrophy and resulting LV cavity dilation [37, 54]. In this investigation, we found that 28 days post-MI, CARD3-overexpressing mice exhibited significantly increased cardiomyocyte cell size and LV hypertrophy, which was associated with impaired contractile function. By contrast, CARD3-deficient mice were shown to be resistant to MI-induced cardiac hypertrophy and LV dysfunction. These observations suggest that these detrimental effects of CARD3 on LV remodelling may be due, at least in part, to pro-hypertrophic effects. In that case, the sustained presence of cytokines also may lead to myocyte phenotype transition and the activation of extracellular matrix, which further augments the remodelling process, including collagen turnover and scar contraction [51]. Therefore, we then examined interstitial fibrosis, an additional key contributor to the development of LV remodelling. Such fibrosis could be attributable to positive regulation of well-known pro-fibrotic factors, such as TGF-β1, collagen I, and collagen III. In support of this hypothesis, Du et al. [5] reported that the specific blockage of CARD3 by MS80 effectively inhibits both collagen synthesis and the excessive proliferation of fibroblasts in pulmonary fibrosis. In summary, our data suggest that CARD3 may positively regulate maladaptive post-MI ventricular remodelling and accelerate heart failure.

As outlined above, underlying the structural and geometric changes of LV remodelling are multiple cellular and molecular events that may occur within heart tissue after MI [9]. Considerable evidence exists to indicate that the activation of the MAPK signalling pathway is of great importance for the process of pathological cardiac remodelling after MI [34]. The MAPK cascade comprises a sequence of successive kinases, including p38, JNKs, and ERKs. In the minutes after experimental MI, ERK1/2, JNK1/2 and p38 MAPK are all activated in both the ischemic myocardium and unaffected portions of the LV of animals [16, 42, 43, 56]. Hence, we evaluated the activation status of the MAPK pathway in our MI models. We found that neither the overexpression nor ablation of CARD3 in infarcted hearts altered the protein levels of phosphorylated MEK-ERK1/2 or JNK1/2 in response to MI. In contrast, p38 levels were greatly enhanced in CARD3-TG mice and reduced in CARD3-KO mice upon MI. Notably, these results are consistent with a previous study, which demonstrated that p38 MAPK activation contributes to progressive LV remodelling post-MI and the transition to heart failure [6]. Importantly, p38 may regulate myocyte apoptosis, inflammation, hypertrophy, and fibroblast proliferation in vitro [44]. The inhibition of p38 or its signalling has been shown to attenuate ventricular damage and remodelling after MI [28, 44]. However, the role of p38 in MI is particularly controversial. Numerous studies have indicated that activation of the p38 pathway plays detrimental roles in MI, while other studies suggest that p38 activation is cardio-protective [52]. Martindale et al. [29] demonstrated that the activation of p38 in the heart led to small heat-shock protein phosphorylation associated with enhanced protection against ischemia/reperfusion injury. The underlying mechanism for the differential function of p38 remains a puzzle. We postulate that it may be related to differences in experimental models, differences in the strain of mice, and differences in time after ischemia. Alternatively, p38 activation appears to be an important step in the translocation and activation of the nuclear transcription factor NF-κB, which in turn may be involved the induction of expression of a variety of stress-inducible genes [30]. In the macrophages of CARD3-deficient mice, the activation of NF-κB and the phosphorylation of the MAPK p38 are impaired in response to stimulation with LPS [49]. In addition to its role in inflammation, the NF-κB signalling pathway has also been shown to be an essential contributor to maladaptive LV remodelling and functional deterioration following MI [36]. Notably, although the extracellular stimuli activated in response to MI may be diverse, there is emerging evidence that these stimuli may converge upon common intracellular pathways to regulate gene expression and protein function [9]. Consequently, involvement of p38 and NF-κB signalling molecules mediated LV remodelling; thus, CARD3 can partly explain the effects of an acute ischemic event. However, we cannot explicitly state whether cross talk exists between p38 and NF-κB pathway in the development of cardiac remodelling after MI. In this regard, further detailed studies are needed to examine the precise role of CARD3 in the process of pathological cardiac remodelling after MI.

In conclusion, the described in vivo and in vitro experiments demonstrate that the overexpression of CARD3 aggravates MI-induced apoptosis, inflammation, hypertrophy, fibrosis, and heart failure via positive regulation of NF-κB and p38 signalling. Conversely, the knockdown of CARD3 mitigates the development of cardiac remodelling after MI. This study on CARD3 may

advance our understanding of the molecular mechanisms underlying MI-triggered cardiac remodelling and thereby provide a new strategy to prevent/treat pathological cardiac remodelling after MI.

Acknowledgments We thank Dr. Richard Flavell (Howard Hughes Medical Institute, Yale University, New Haven, Connecticut) for providing the CARD3-KO mice. We thank Rui Zhang, Xueyong Zhu, Zhangli Li, Ya Deng, Yan Zhang and Xin Zhang for providing experimental technological assistance. Dr. Xin Chen is a fellow at the Collaborative Innovation Center for Cardiovascular Disease Translational Medicine. This study was supported by grants from the National Natural Science Foundation of China (No. 81370259), the Natural Science Foundation for Young Scientists of Jiangsu Province (No. BK20150093), and the 333 project in Jiangsu Province (2015).

Compliance with ethical standards

Conflict of interest The authors declare that they have no conflict of interest.

References

1. Abe J, Baines CP, Berk BC (2000) Role of mitogen-activated protein kinases in ischemia and reperfusion injury: the good and the bad. Circ Res 86:607–609
2. Chandrashekhar Y, Sen S, Anway R, Shuros A, Anand I (2004) Long-term caspase inhibition ameliorates apoptosis, reduces myocardial troponin-I cleavage, protects left ventricular function, and attenuates remodeling in rats with myocardial infarction. J Am Coll Cardiol 43:295–301
3. Chen K, Gao L, Liu Y, Zhang Y, Jiang DS, Wei X, Zhu XH, Zhang R, Chen Y, Yang Q, Kioka N, Zhang XD, Li H (2013) Vinexin-beta protects against cardiac hypertrophy by blocking the Akt-dependent signalling pathway. Basic Res Cardiol 108:338. doi:10.1007/s00395-013-0338-0
4. Dorn GW 2nd (2009) Apoptotic and non-apoptotic programmed cardiomyocyte death in ventricular remodelling. Cardiovasc Res 81:465–473. doi:10.1093/cvr/cvn243
5. Du X, Jiang S, Liu H, Xin X, Li J, Geng M, Jiang H (2010) MS80, a novel sulfated polysaccharide, inhibits CD40-NF-kappaB pathway via targeting RIP2. Mol Cell Biochem 337:277–285. doi:10.1007/s11010-009-0309-9
6. Engelbrecht AM, Niesler C, Page C, Lochner A (2004) p38 and JNK have distinct regulatory functions on the development of apoptosis during simulated ischaemia and reperfusion in neonatal cardiomyocytes. Basic Res Cardiol 99:338–350. doi:10.1007/s00395-004-0478-3
7. Feuerstein GZ, Young PR (2000) Apoptosis in cardiac diseases: stress- and mitogen-activated signaling pathways. Cardiovasc Res 45:560–569
8. Frangogiannis NG (2014) The immune system and the remodeling infarcted heart: cell biological insights and therapeutic opportunities. J Cardiovasc Pharmacol 63:185–195. doi:10.1097/FJC.0000000000000003
9. Gajarsa JJ, Kloner RA (2011) Left ventricular remodeling in the post-infarction heart: a review of cellular, molecular mechanisms, and therapeutic modalities. Heart Fail Rev 16:13–21. doi:10.1007/s10741-010-9181-7
10. Gallagher G, Menzie S, Huang Y, Jackson C, Hunyor SN (2007) Regional cardiac dysfunction is associated with specific alterations in inflammatory cytokines and matrix metalloproteinases after acute myocardial infarction in sheep. Basic Res Cardiol 102:63–72. doi:10.1007/s00395-006-0610-7
11. Go AS, Mozaffarian D, Roger VL, Benjamin EJ, Berry JD, Blaha MJ, Dai S, Ford ES, Fox CS, Franco S, Fullerton HJ, Gillespie C, Hailpern SM, Heit JA, Howard VJ, Huffman MD, Judd SE, Kissela BM, Kittner SJ, Lackland DT, Lichtman JH, Lisabeth LD, Mackey RH, Magid DJ, Marcus GM, Marelli A, Matchar DB, McGuire DK, Mohler ER, 3rd, Moy CS, Mussolino ME, Neumar RW, Nichol G, Pandey DK, Paynter NP, Reeves MJ, Sorlie PD, Stein J, Towfighi A, Turan TN, Virani SS, Wong ND, Woo D, Turner MB, American Heart Association Statistics C, Stroke Statistics S (2014) Heart disease and stroke statistics–2014 update: a report from the American Heart Association. Circulation 129:e28–e292. doi:10.1161/01.cir.0000441139.02102.80
12. Gottlieb RA (2003) Mitochondrial signaling in apoptosis: mitochondrial daggers to the breaking heart. Basic Res Cardiol 98:242–249. doi:10.1007/s00395-003-0404-0
13. Heusch G (2013) Cardioprotection: chances and challenges of its translation to the clinic. Lancet 381:166–175. doi:10.1016/S0140-6736(12)60916-7
14. Heusch G, Kleinbongard P, Skyschally A (2013) Myocardial infarction and coronary microvascular obstruction: an intimate, but complicated relationship. Basic Res Cardiol 108:380. doi:10.1007/s00395-013-0380-y
15. Heusch G, Libby P, Gersh B, Yellon D, Bohm M, Lopaschuk G, Opie L (2014) Cardiovascular remodelling in coronary artery disease and heart failure. Lancet 383:1933–1943. doi:10.1016/S0140-6736(14)60107-0
16. Heusch P, Canton M, Aker S, van de Sand A, Konietzka I, Rassaf T, Menazza S, Brodde OE, Di Lisa F, Heusch G, Schulz R (2010) The contribution of reactive oxygen species and p38 mitogen-activated protein kinase to myofilament oxidation and progression of heart failure in rabbits. Br J Pharmacol 160:1408–1416. doi:10.1111/j.1476-5381.2010.00793.x
17. Hollenbach E, Neumann M, Vieth M, Roessner A, Malfertheiner P, Naumann M (2004) Inhibition of p38 MAP kinase- and RICK/NF-kappaB-signaling suppresses inflammatory bowel disease. FASEB J 18:1550–1552. doi:10.1096/fj.04-1642fje
18. Inohara N, Koseki T, Lin J, del Peso L, Lucas PC, Chen FF, Ogura Y, Nunez G (2000) An induced proximity model for NF-kappa B activation in the Nod1/RICK and RIP signaling pathways. J Biol Chem 275:27823–27831. doi:10.1074/jbc.M003415200
19. Jacquet S, Nishino Y, Kumphune S, Sicard P, Clark JE, Kobayashi KS, Flavell RA, Eickhoff J, Cotten M, Marber MS (2008) The role of RIP2 in p38 MAPK activation in the stressed heart. J Biol Chem 283:11964–11971. doi:10.1074/jbc.M707750200
20. Jiang DS, Li L, Huang L, Gong J, Xia H, Liu X, Wan N, Wei X, Zhu X, Chen Y, Chen X, Zhang XD, Li H (2014) Interferon regulatory factor 1 is required for cardiac remodeling in response to pressure overload. Hypertension 64:77–86. doi:10.1161/HYPERTENSIONAHA.114.03229
21. Kobayashi K, Inohara N, Hernandez LD, Galan JE, Nunez G, Janeway CA, Medzhitov R, Flavell RA (2002) RICK/Rip2/CARDIAK mediates signalling for receptors of the innate and adaptive immune systems. Nature 416:194–199. doi:10.1038/416194a
22. Landmesser U, Wollert KC, Drexler H (2009) Potential novel pharmacological therapies for myocardial remodelling. Cardiovasc Res 81:519–527. doi:10.1093/cvr/cvn317
23. Levin MC, Jirholt P, Wramstedt A, Johansson ME, Lundberg AM, Trajkovska MG, Stahlman M, Fogelstrand P, Brisslert M, Fogelstrand L, Yan ZQ, Hansson GK, Bjorkbacka H, Olofsson SO, Boren J (2011) Rip2 deficiency leads to increased

atherosclerosis despite decreased inflammation. Circ Res 109:1210–1218. doi:10.1161/CIRCRESAHA.111.246702
24. Li HL, Zhuo ML, Wang D, Wang AB, Cai H, Sun LH, Yang Q, Huang Y, Wei YS, Liu PP, Liu DP, Liang CC (2007) Targeted cardiac overexpression of A20 improves left ventricular performance and reduces compensatory hypertrophy after myocardial infarction. Circulation 115:1885–1894. doi:10.1161/CIRCULATIONAHA.106.656835
25. Li L, Chen W, Zhu Y, Wang X, Jiang DS, Huang F, Wang L, Xiang F, Qin W, Wang Q, Zhang R, Zhu X, Li H, Chen X (2014) Caspase recruitment domain 6 protects against cardiac hypertrophy in response to pressure overload. Hypertension 64:94–102. doi:10.1161/HYPERTENSIONAHA.113.03021
26. Li S, Zhong S, Zeng K, Luo Y, Zhang F, Sun X, Chen L (2010) Blockade of NF-kappaB by pyrrolidine dithiocarbamate attenuates myocardial inflammatory response and ventricular dysfunction following coronary microembolization induced by homologous microthrombi in rats. Basic Res Cardiol 105:139–150. doi:10.1007/s00395-009-0067-6
27. Lu J, Bian ZY, Zhang R, Zhang Y, Liu C, Yan L, Zhang SM, Jiang DS, Wei X, Zhu XH, Chen M, Wang AB, Chen Y, Yang Q, Liu PP, Li H (2013) Interferon regulatory factor 3 is a negative regulator of pathological cardiac hypertrophy. Basic Res Cardiol 108:326. doi:10.1007/s00395-012-0326-9
28. Marber MS, Rose B, Wang Y (2011) The p38 mitogen-activated protein kinase pathway–a potential target for intervention in infarction, hypertrophy, and heart failure. J Mol Cell Cardiol 51:485–490. doi:10.1016/j.yjmcc.2010.10.021
29. Martindale JJ, Wall JA, Martinez-Longoria DM, Aryal P, Rockman HA, Guo Y, Bolli R, Glembotski CC (2005) Overexpression of mitogen-activated protein kinase kinase 6 in the heart improves functional recovery from ischemia in vitro and protects against myocardial infarction in vivo. J Biol Chem 280:669–676. doi:10.1074/jbc.M406690200
30. Maulik N, Sato M, Price BD, Das DK (1998) An essential role of NFkappaB in tyrosine kinase signaling of p38 MAP kinase regulation of myocardial adaptation to ischemia. FEBS Lett 429:365–369
31. McCain ML, Sheehy SP, Grosberg A, Goss JA, Parker KK (2013) Recapitulating maladaptive, multiscale remodeling of failing myocardium on a chip. Proc Natl Acad Sci USA 110:9770–9775. doi:10.1073/pnas.1304913110
32. McCarthy JV, Ni J, Dixit VM (1998) RIP2 is a novel NF-kappaB-activating and cell death-inducing kinase. J Biol Chem 273:16968–16975
33. Munz B, Hildt E, Springer ML, Blau HM (2002) RIP2, a checkpoint in myogenic differentiation. Mol Cell Biol 22:5879–5886
34. Muslin AJ (2008) MAPK signalling in cardiovascular health and disease: molecular mechanisms and therapeutic targets. Clin Sci Lond 115:203–218. doi:10.1042/CS20070430
35. Nian M, Lee P, Khaper N, Liu P (2004) Inflammatory cytokines and postmyocardial infarction remodeling. Circ Res 94:1543–1553. doi:10.1161/01.RES.0000130526.20854.fa
36. Onai Y, Suzuki J, Maejima Y, Haraguchi G, Muto S, Itai A, Isobe M (2007) Inhibition of NF-{kappa}B improves left ventricular remodeling and cardiac dysfunction after myocardial infarction. Am J Physiol Heart Circ Physiol 292:H530–H538. doi:10.1152/ajpheart.00549.2006
37. Opie LH, Commerford PJ, Gersh BJ, Pfeffer MA (2006) Controversies in ventricular remodelling. Lancet 367:356–367. doi:10.1016/S0140-6736(06)68074-4
38. Park JH, Kim YG, McDonald C, Kanneganti TD, Hasegawa M, Body-Malapel M, Inohara N, Nunez G (2007) RICK/RIP2 mediates innate immune responses induced through Nod1 and Nod2 but not TLRs. J Immunol 178:2380–2386
39. Penna C, Perrelli MG, Pagliaro P (2013) Mitochondrial pathways, permeability transition pore, and redox signaling in cardioprotection: therapeutic implications. Antioxid Redox Signal 18:556–599. doi:10.1089/ars.2011.4459
40. Prech M, Marszalek A, Schroder J, Filas V, Lesiak M, Jemielity M, Araszkiewicz A, Grajek S (2010) Apoptosis as a mechanism for the elimination of cardiomyocytes after acute myocardial infarction. Am J Cardiol 105:1240–1245. doi:10.1016/j.amjcard.2009.12.039
41. Rahman MA, Sundaram K, Mitra S, Gavrilin MA, Wewers MD (2014) Receptor interacting protein-2 plays a critical role in human lung epithelial cells survival in response to Fas-induced cell-death. PLoS One 9:e92731. doi:10.1371/journal.pone.0092731
42. Ren J, Zhang S, Kovacs A, Wang Y, Muslin AJ (2005) Role of p38alpha MAPK in cardiac apoptosis and remodeling after myocardial infarction. J Mol Cell Cardiol 38:617–623. doi:10.1016/j.yjmcc.2005.01.012
43. Schulz R, Aker S, Belosjorow S, Konietzka I, Rauen U, Heusch G (2003) Stress kinase phosphorylation is increased in pacing-induced heart failure in rabbits. Am J Physiol Heart Circ Physiol 285:H2084–H2090. doi:10.1152/ajpheart.01038.2002
44. See F, Thomas W, Way K, Tzanidis A, Kompa A, Lewis D, Itescu S, Krum H (2004) p38 mitogen-activated protein kinase inhibition improves cardiac function and attenuates left ventricular remodeling following myocardial infarction in the rat. J Am Coll Cardiol 44:1679–1689. doi:10.1016/j.jacc.2004.07.038
45. Sicard P, Jacquet S, Kobayashi KS, Flavell RA, Marber MS (2009) Pharmacological postconditioning effect of muramyl dipeptide is mediated through RIP2 and TAK1. Cardiovasc Res 83:277–284. doi:10.1093/cvr/cvp055
46. Sutton MG, Sharpe N (2000) Left ventricular remodeling after myocardial infarction: pathophysiology and therapy. Circulation 101:2981–2988
47. Tang TT, Yuan J, Zhu ZF, Zhang WC, Xiao H, Xia N, Yan XX, Nie SF, Liu J, Zhou SF, Li JJ, Yao R, Liao MY, Tu X, Liao YH, Cheng X (2012) Regulatory T cells ameliorate cardiac remodeling after myocardial infarction. Basic Res Cardiol 107:232. doi:10.1007/s00395-011-0232-6
48. Timmers L, van Keulen JK, Hoefer IE, Meijs MF, van Middelaar B, den Ouden K, van Echteld CJ, Pasterkamp G, de Kleijn DP (2009) Targeted deletion of nuclear factor kappaB p50 enhances cardiac remodeling and dysfunction following myocardial infarction. Circ Res 104:699–706. doi:10.1161/CIRCRESAHA.108.189746
49. Usluoglu N, Pavlovic J, Moelling K, Radziwill G (2007) RIP2 mediates LPS-induced p38 and IkappaBalpha signaling including IL-12 p40 expression in human monocyte-derived dendritic cells. Eur J Immunol 37:2317–2325. doi:10.1002/eji.200636388
50. Valen G (2004) Signal transduction through nuclear factor kappa B in ischemia-reperfusion and heart failure. Basic Res Cardiol 99:1–7. doi:10.1007/s00395-003-0442-7
51. van den Borne SW, Diez J, Blankesteijn WM, Verjans J, Hofstra L, Narula J (2010) Myocardial remodeling after infarction: the role of myofibroblasts. Nat Rev Cardiol 7:30–37. doi:10.1038/nrcardio.2009.199
52. Wang Y (2007) Mitogen-activated protein kinases in heart development and diseases. Circulation 116:1413–1423. doi:10.1161/CIRCULATIONAHA.106.679589
53. Xiao J, Moon M, Yan L, Nian M, Zhang Y, Liu C, Lu J, Guan H, Chen M, Jiang D, Jiang H, Liu PP, Li H (2012) Cellular FLICE-inhibitory protein protects against cardiac remodelling after myocardial infarction. Basic Res Cardiol 107:239. doi:10.1007/s00395-011-0239-z
54. Yang F, Liu YH, Yang XP, Xu J, Kapke A, Carretero OA (2002) Myocardial infarction and cardiac remodelling in mice. Exp Physiol 87:547–555

55. Yin X, Krikorian P, Logan T, Csizmadia V (2010) Induction of RIP-2 kinase by proinflammatory cytokines is mediated via NF-kappaB signaling pathways and involves a novel feed-forward regulatory mechanism. Mol Cell Biochem 333:251–259. doi:10.1007/s11010-009-0226-y
56. Yoshida K, Yoshiyama M, Omura T, Nakamura Y, Kim S, Takeuchi K, Iwao H, Yoshikawa J (2001) Activation of mitogen-activated protein kinases in the non-ischemic myocardium of an acute myocardial infarction in rats. Jpn Circ J 65:808–814
57. Youle RJ, Strasser A (2008) The BCL-2 protein family: opposing activities that mediate cell death. Nat Rev Mol Cell Biol 9:47–59. doi:10.1038/nrm2308
58. Zhang WH, Wang X, Narayanan M, Zhang Y, Huo C, Reed JC, Friedlander RM (2003) Fundamental role of the Rip2/caspase-1 pathway in hypoxia and ischemia-induced neuronal cell death. Proc Natl Acad Sci USA 100:16012–16017. doi:10.1073/pnas.2534856100
59. Zhang Y, Liu X, She ZG, Jiang DS, Wan N, Xia H, Zhu XH, Wei X, Zhang XD, Li H (2014) Interferon regulatory factor 9 is an essential mediator of heart dysfunction and cell death following myocardial ischemia/reperfusion injury. Basic Res Cardiol 109:434. doi:10.1007/s00395-014-0434-9